ORIGINAL ARTICLE

Traveling waves in a coarse-grained model of volume-filling cell invasion: Simulations and comparisons

Rebecca M. Crossley[1] ![ORCID] | Philip K. Maini[1] | Tommaso Lorenzi[2] |
Ruth E. Baker[1]

[1]Mathematical Institute, University of Oxford, Oxford, UK

[2]Department of Mathematical Sciences "G. L. Lagrange,", Politecnico di Torino, Torino, Italy

Correspondence
Rebecca M. Crossley, Mathematical
Institute, University of Oxford, Oxford
OX2 6GG, UK.
Email: rebecca.crossley@maths.ox.ac.uk

Abstract

Many reaction–diffusion models produce traveling wave solutions that can be interpreted as waves of invasion in biological scenarios such as wound healing or tumor growth. These partial differential equation models have since been adapted to describe the interactions between cells and extracellular matrix (ECM), using a variety of different underlying assumptions. In this work, we derive a system of reaction–diffusion equations, with cross-species density-dependent diffusion, by coarse-graining an agent-based, volume-filling model of cell invasion into ECM. We study the resulting traveling wave solutions both numerically and analytically across various parameter regimes. Subsequently, we perform a systematic comparison between the behaviors observed in this model and those predicted by simpler models in the literature that do not take into account volume-filling effects in the same way. Our study justifies the use of some of these simpler, more analytically tractable models in reproducing the qualitative properties of the

solutions in some parameter regimes, but it also reveals some interesting properties arising from the introduction of cell and ECM volume-filling effects, where standard model simplifications might not be appropriate.

1 | INTRODUCTION

Cell invasion is central to a variety of biological phenomena, playing a key role in morphogenesis, tumor growth, and tissue engineering. Many different mathematical approaches have been used to model cell invasion processes, from agent-based models describing the processes underlying invasion at a single-cell level, to partial differential equation (PDE) models that provide a cell population-level description of invasion in terms of cell density dynamics.[1] While some of these PDE models have been formulated through adaptations of classical models for invasion processes in other biological contexts, many are derived by coarse-graining a cell-level description to produce PDEs that offer the corresponding population-level description. However, there remain a number of unanswered questions regarding the specific choice of model for a given application, including how varying assumptions in the agent-based model give rise to different PDE models and to what extent these differences impact the cell population-level description.[2]

In this work, the impact of various modeling assumptions at the single-cell level is compared by investigating the qualitative and quantitative properties of the solutions of the resulting PDE models. In particular, since in many real-life instances of cell invasion, the cells have to invade through extracellular matrix (ECM)[3–5]—that is, the network of proteins and other molecules that impact collective cell invasion by reducing space available for cells to migrate into—the focus is on models of cell invasion into ECM.

The classic example of a model describing invasion of a single population is the Fisher–Kolmogorov–Pietrovskii–Piskunov (FKPP) model, which was first proposed in the context of the spread of an advantageous gene.[6,7] This model has seen a broad spectrum of applications in the natural sciences: most notably in cell biology[8,9] and ecology,[10,11] where traveling wave solutions are representative of invasion phenomena.[12,13] A model of cell invasion through ECM is presented in El-Hachem et al.[14] This consists of a system of two coupled PDEs, with a nonlinear cross-species density-dependent diffusion term and logistic growth, whereby proliferation of the cell population is limited by the presence of cells and ECM. A similar model is considered in Colson et al.,[15] where proliferation depends only on the presence of cells. An obvious question to ask is how the predictions of such models may be affected by a consistent description of the role of volume-filling effects (i.e., cells and ECM take up some given volume, preventing cell invasion) across both proliferative and diffusive mechanisms of cell dynamics. In particular, the impact of crowding on cell motility is generally modeled at a population-level by the introduction of a density-dependent diffusion term, such as in Refs. [16–19]. However, these models provide a phenomenological description of the impact of crowding, rather than considering how interactions at the individual cell-level directly impact motility at the population-level.

This study aims to extend and apply the work in Simpson et al.[20,21] to develop an agent-based model for cell invasion into ECM, taking into account volume-filling effects, where both cell motility and proliferation are impacted by the presence of other cells or ECM components. We make the simplifying assumption that space is the only factor limiting cell invasion, whereas other models in the literature[22,23] assume various other factors, such as nutrient-limited growth.[24] By coarse-graining this model, a limiting PDE description is formally derived and explored both analytically and numerically, making it possible to carry out a systematic comparison between the population-level behaviors observed in this model and those predicted by simpler models. In particular, we compare how the population-level behaviors predicted by this model relate to existing models built on different constitutive assumptions, such as the FKPP model, or the simpler models presented in Refs. [14, 15]. Each of these simpler models can be recovered from the model presented in this work by neglecting specific terms, such as those capturing volume-filling effects.

2 | MATHEMATICAL MODEL AND PRELIMINARY RESULTS

We begin by developing a simple one-dimensional, on-lattice, agent-based model of cell invasion into ECM that incorporates both cell motility and proliferation, and degradation of ECM, in the presence of volume-filling effects. We then coarse-grain this model to formally derive a corresponding PDE model that comprises a system of coupled PDEs for the densities of cells and ECM.[20,25]

2.1 | Agent-based model

In the simplified setting of this model, cells are represented as discrete agents that can proliferate and move on a one-dimensional uniform lattice, which constitutes the spatial domain and can also degrade the surrounding ECM, which is regarded as being composed of discrete constitutive elements. The novel aspect of this model is the introduction of volume-filling effects, similar to the model described in Morris et al.,[26] which uses the methods described in Painter and Hillen,[27] but extended to multiple populations.[21]

Let the number of cells and ECM elements on lattice site $i = 1, 2, \ldots$ of width Δ at time $\tilde{t} \in \mathbb{R}^+$ of realization $j = 1, 2, \ldots, J$ of the model be denoted, respectively, by $u_i^j(\tilde{t})$ and $m_i^j(\tilde{t})$. We assume that ECM elements have constant density and are chosen to occupy a volume equal to that of a cell, such that at most N cells or ECM elements can occupy each lattice site.

The dynamics of the cells are governed by two mechanisms: proliferation, in which a cell places a daughter cell into the same lattice site it occupies; and motility, whereby cells can move to one of their two adjacent lattice sites. Moreover, ECM elements can be degraded by cells in the same lattice site as them. To incorporate volume-filling effects into the model, we prescribe that each lattice site has a maximum occupancy level N,[28] and we assume that

(A1) if a cell attempts a move to a neighboring lattice site, then the probability that the move is successful decreases linearly with the occupancy level of the target site, such that the probability of a successful move to a target site with occupancy level N is zero;

(A2) if a cell attempts to proliferate, then the probability of success decreases linearly with the occupancy level of the site where the cell is located, such that the probability of a successful proliferation event in a site with occupancy level N is zero.

Probability of cell movement

A cell attempts a movement in a time step τ with probability $p_\mathrm{m} \in [0, 1]$, and the attempted movement from lattice site i to either of the neighboring lattice sites $i \pm 1$ occurs with equal probability $1/2$. Using Assumption 2.1, we can define the probability of movement to the left, $T_{i-}^{\mathrm{m}^j}(\tilde{t})$, or right, $T_{i+}^{\mathrm{m}^j}(\tilde{t})$, during the time interval $[\tilde{t}, \tilde{t} + \tau)$ of realization j, as

$$T_{i\pm}^{\mathrm{m}^j}(\tilde{t}) = \frac{p_\mathrm{m}}{2}\left(1 - \frac{u_{i\pm1}^j(\tilde{t}) + m_{i\pm1}^j(\tilde{t})}{N}\right). \tag{1}$$

Probability of cell proliferation

A cell in lattice site i attempts to proliferate in time step τ with probability $p_\mathrm{p} \in [0, 1]$. If proliferation occurs, then the cell places a daughter cell into the same lattice site as itself. Using Assumption 2.1, we can define the probability of proliferation, $T_i^{\mathrm{p}^j}(\tilde{t})$, during the time interval $[\tilde{t}, \tilde{t} + \tau)$ of realization j, as

$$T_i^{\mathrm{p}^j}(\tilde{t}) = p_\mathrm{p}\left(1 - \frac{u_i^j(\tilde{t}) + m_i^j(\tilde{t})}{N}\right). \tag{2}$$

Note that, the initial distributions of cells and ECM elements must be such that at most N cells or ECM elements can occupy each lattice site to ensure the probabilities $T_{i\pm}^{\mathrm{m}^j}(\tilde{t})$, $T_i^{\mathrm{p}^j}(\tilde{t}) \geq 0$ are well-defined. Under the assumption that the initial distributions of cells and ECM elements satisfy $0 \leq u_i^j(0) + m_i^j(0) \leq N$ for all $j = 1, 2, \ldots, J$ and $i = 1, 2, \ldots$, the definitions for the probabilities of cell movement and proliferation given by Equations (1) and (2) ensure that

$$0 \leq u_i^j(\tilde{t}) + m_i^j(\tilde{t}) \leq N \quad \text{for all} \quad j = 1, 2, \ldots, J \quad \text{and} \quad i = 1, 2, \ldots \quad \text{for any} \quad \tilde{t} \in \mathbb{R}^+. \tag{3}$$

Probability of ECM degradation

During the time interval $[\tilde{t}, \tilde{t} + \tau)$ of realization j, an element of ECM in lattice site i is degraded by a cell on the same lattice site with probability $p_\mathrm{d} \in [0, 1]$, such that the degradation per unit element of ECM, $T_i^{\mathrm{d}^j}(\tilde{t})$, is

$$T_i^{\mathrm{d}^j}(\tilde{t}) = p_\mathrm{d} u_i^j(\tilde{t}). $$

2.2 | Corresponding coarse-grained model

In order to derive a coarse-grained description of the agent-based model, we introduce the average occupancy of lattice site i at time $\tilde{t}$ by cells and ECM elements over J realizations of the model, denoted, respectively, by

$$\langle u_i(\tilde{t}) \rangle = \frac{1}{J}\sum_{j=1}^J u_i^j(\tilde{t}) \quad \text{and} \quad \langle m_i(\tilde{t}) \rangle = \frac{1}{J}\sum_{j=1}^J m_i^j(\tilde{t}).$$

Coarse-grained model of cell dynamics

We proceed to derive a coarse-grained model by considering how the average occupancy in lattice site i changes during the time interval $[\tilde{t}, \tilde{t} + \tau)$:

$$
\begin{aligned}
\langle u_i(\tilde{t} + \tau)\rangle =& \langle u_i(\tilde{t})\rangle \\
&+ \frac{p_{\mathrm{m}}}{2}\langle u_{i+1}(\tilde{t})\rangle \left(1 - \frac{\langle u_i(\tilde{t})\rangle + \langle m_i(\tilde{t})\rangle}{N}\right) \\
&+ \frac{p_{\mathrm{m}}}{2}\langle u_{i-1}(\tilde{t})\rangle \left(1 - \frac{\langle u_i(\tilde{t})\rangle + \langle m_i(\tilde{t})\rangle}{N}\right) \\
&- \frac{p_{\mathrm{m}}}{2}\langle u_i(\tilde{t})\rangle \left(1 - \frac{\langle u_{i+1}(\tilde{t})\rangle + \langle m_{i+1}(\tilde{t})\rangle}{N}\right) \\
&- \frac{p_{\mathrm{m}}}{2}\langle u_i(\tilde{t})\rangle \left(1 - \frac{\langle u_{i-1}(\tilde{t})\rangle + \langle m_{i-1}(\tilde{t})\rangle}{N}\right) \\
&+ p_{\mathrm{p}}\langle u_i(\tilde{t})\rangle \left(1 - \frac{\langle u_i(\tilde{t})\rangle + \langle m_i(\tilde{t})\rangle}{N}\right).
\end{aligned}
\tag{4}
$$

Note that, in writing down Equation (4) we have used probabilistic approximations of the mean-field type which are frequently used for the coarse-graining of agent-based models and involve assuming independence of lattice sites (see, e.g., Penington et al.[29]). Rearranging Equation (4) and dividing both sides by τ yields

$$
\begin{aligned}
\frac{\langle u_i(\tilde{t} + \tau)\rangle - \langle u_i(\tilde{t})\rangle}{\tau} =& \frac{p_{\mathrm{m}}\Delta^2}{2\tau}\left[\frac{\langle u_{i-1}(\tilde{t})\rangle - 2\langle u_i(\tilde{t})\rangle + \langle u_{i+1}(\tilde{t})\rangle}{\Delta^2}\right] \\
&+ \frac{p_{\mathrm{m}}\Delta^2}{2\tau N}\left[\frac{\langle u_i(\tilde{t})\rangle(\langle m_{i-1}(\tilde{t})\rangle - 2\langle m_i(\tilde{t})\rangle + \langle m_{i+1}(\tilde{t})\rangle)}{\Delta^2}\right] \\
&- \frac{p_{\mathrm{m}}\Delta^2}{2\tau N}\left[\frac{\langle m_i(\tilde{t})\rangle(\langle u_{i-1}(\tilde{t})\rangle - 2\langle u_i(\tilde{t})\rangle + \langle u_{i+1}(\tilde{t})\rangle)}{\Delta^2}\right] \\
&+ \frac{p_{\mathrm{p}}}{\tau}\langle u_i(\tilde{t})\rangle \left(1 - \frac{\langle u_i(\tilde{t})\rangle + \langle m_i(\tilde{t})\rangle}{N}\right).
\end{aligned}
\tag{5}
$$

We now divide both sides of Equation (5) by length scale Δ, perform a Taylor expansion, and take limits as $\Delta, \tau \to 0$ to obtain a description of the cell density dynamics in terms of the variables $\tilde{u}(\tilde{x}, \tilde{t})$ and $\tilde{m}(\tilde{x}, \tilde{t})$, that are the continuum counterparts of $\langle u_i(\tilde{t})\rangle/\Delta$ and $\langle m_i(\tilde{t})\rangle/(\mu\Delta)$ that represent, respectively, the number density of cells and the density of ECM at position $\tilde{x} \in \mathbb{R}$ and time $\tilde{t} \in (0, \infty)$. The factor μ represents the number of cells equivalent to a unit mass of ECM and is introduced as a conversion factor between the density of ECM, as defined by mass of ECM per unit volume, and the number density of ECM elements, given by $\mu\tilde{m}(\tilde{x}, \tilde{t})$. Under the assumptions

$$
\lim_{\Delta, \tau \to 0} \frac{p_{\mathrm{m}}\Delta^2}{2\tau} = \tilde{D}, \qquad \lim_{\tau \to 0} \frac{p_{\mathrm{p}}}{\tau} = \tilde{r}, \qquad \lim_{\Delta \to 0} \frac{N}{\Delta} = \tilde{K},
\tag{6}
$$

we obtain the following PDE for the cell density $\tilde{u}(\tilde{x}, \tilde{t})$:

$$\frac{\partial \tilde{u}}{\partial \tilde{t}} = \tilde{D} \frac{\partial}{\partial \tilde{x}} \left[\left(1 - \frac{\tilde{u} + \tilde{\mu}\tilde{m}}{\tilde{K}} \right) \frac{\partial \tilde{u}}{\partial \tilde{x}} + \tilde{u} \frac{\partial}{\partial \tilde{x}} \left(\frac{\tilde{u} + \tilde{\mu}\tilde{m}}{\tilde{K}} \right) \right] + \tilde{r}\tilde{u} \left(1 - \frac{\tilde{u} + \tilde{\mu}\tilde{m}}{\tilde{K}} \right), \tag{7}$$

where $\tilde{x} \in \mathbb{R}$ and $\tilde{t} \in (0, \infty)$. Note that the first term on the right-hand side of Equation (7) describes the movement of cells down gradients in cell density, with movement prevented by the presence of surrounding cells and ECM, as expected by the introduction of volume-filling effects. The second term models the motion of the cells down the "total density gradient" of cells and ECM, $\tilde{u} + \tilde{\mu}\tilde{m}$. The third term captures cell proliferation, which is also impacted by volume-filling effects. From Equation (7), it is clear that the parameter $\tilde{D} \geq 0$, which is defined via Equation (6), can be regarded as the diffusion coefficient of the cells in the absence of ECM, while the parameters $\tilde{r} \geq 0$ and $\tilde{K} > 0$, which are also defined via Equation (6), are the intrinsic growth rate of the cell population, and the density corresponding to the maximum occupancy level (i.e., the carrying capacity), respectively.

Coarse-grained model of ECM dynamics
Probabilistic approximations similar to those underlying Equation (4) give the following conservation equation for the evolution of ECM elements in lattice site i during the time interval $[\tilde{t}, \tilde{t} + \tau)$:

$$\langle m_i(\tilde{t} + \tau) \rangle = \langle m_i(\tilde{t}) \rangle - p_d \langle u_i(\tilde{t}) \rangle \langle m_i(\tilde{t}) \rangle. \tag{8}$$

Rearranging Equation (8), dividing by Δ and τ and taking limits as $\Delta, \tau \to 0$, under the assumption

$$\lim_{\Delta, \tau \to 0} \frac{p_d \Delta}{\tau} = \tilde{\lambda}, \tag{9}$$

we formally obtain the following differential equation for ECM density $\tilde{m}(\tilde{x}, \tilde{t})$:

$$\frac{\partial \tilde{m}}{\partial \tilde{t}} = -\tilde{\lambda}\tilde{m}\tilde{u}, \tag{10}$$

where $\tilde{x} \in \mathbb{R}$ and $\tilde{t} \in (0, \infty)$. Here, the parameter $\tilde{\lambda} \geq 0$ defined via Equation (9) is the per cell degradation rate of ECM.

We observe that when there is no ECM degradation (i.e., if $\tilde{\lambda} = 0$) and ECM is uniformly distributed at $\tilde{t} = 0$ (i.e. if $\tilde{m}(\tilde{x}, 0) \equiv \tilde{m}^0$ where $\tilde{m}^0 \in \mathbb{R}^+$ with $0 \leq \tilde{m}^0 \leq \tilde{K}$), the mathematical model defined via Equations (7) and (10) simplifies to the following FKPP model of cell dynamics[6]:

$$\frac{\partial \tilde{u}}{\partial \tilde{t}} = \hat{D} \frac{\partial^2 \tilde{u}}{\partial \tilde{x}^2} + \hat{r}\tilde{u} \left(1 - \frac{\tilde{u}}{\hat{K}} \right), \tag{11}$$

where

$$\hat{D} = \left(1 - \frac{\tilde{\mu}\tilde{m}^0}{\tilde{K}} \right) \tilde{D}, \quad \hat{r} = \left(1 - \frac{\tilde{\mu}\tilde{m}^0}{\tilde{K}} \right) \tilde{r}, \quad \hat{K} = \left(1 - \frac{\tilde{\mu}\tilde{m}^0}{\tilde{K}} \right) \tilde{K}.$$

2.3 | Nondimensional coarse-grained model

The mathematical model defined via Equations (7) and (10) can be nondimensionalized by the introduction of the following nondimensional variables

$$u = \frac{\tilde{u}}{\tilde{K}}, \quad m = \frac{\tilde{\mu}\tilde{m}}{\tilde{K}}, \quad t = \tilde{t}\tilde{r}, \quad x = \sqrt{\frac{\tilde{r}}{\tilde{D}}}\tilde{x},$$

and written as

$$\frac{\partial u}{\partial t} = \frac{\partial}{\partial x}\left[(1-m)\frac{\partial u}{\partial x} + u\frac{\partial m}{\partial x}\right] + u(1-u-m), \tag{12}$$

$$\frac{\partial m}{\partial t} = -\lambda mu, \tag{13}$$

where $x \in \mathbb{R}$ and $t \in (0, \infty)$. Here, the only remaining parameter is $\lambda = \tilde{\lambda}\tilde{K}/\tilde{r} \geq 0$, which is interpreted as the rescaled ECM degradation rate. We complement the model defined via Equations (12) and (13) with no flux boundary conditions for Equation (12):

$$(1-m)\frac{\partial u}{\partial x} + u\frac{\partial m}{\partial x} = 0\bigg|_{x=0}, \tag{14}$$

and $u, \partial u/\partial x \to 0$ as $x \to \infty$. We also have the following initial conditions:

$$u(x,0) = u_0(x) \geq 0, \quad m(x,0) = m_0(x) \geq 0, \quad 0 \leq u_0(x) + m_0(x) \leq 1 \quad \forall x \in \mathbb{R}. \tag{15}$$

We note that by assuming at the single-cell level that both the presence of cells and ECM elements impair the movement and proliferation of the cells, the resulting population-level description for cell density evolution in Equation (12) exhibits a number of differences to similar models without volume-filling effects. For example, the model studied by El Hachem et al.[14] does not consider volume-filling of cells to impair cell movement, and therefore contains one less flux term, namely that accounting for movement of cells down the "total density gradient." This model can be recovered from Equation (12) by employing different underlying assumptions such that the probability of movement depends on the average available space (where space is only filled by ECM) between the target lattice site and the lattice site the cell occupies at time $\tilde{t}$.

2.4 | Numerical exploration of possible traveling wave solutions

We are interested in the possible constant profile, constant speed traveling wave solutions displayed by the model defined via Equations (12) and (13). As such, we first explore the range of possible behaviors numerically. We report on the results of numerical simulations carried out for the model posed on the spatial domain $(0, L)$, with $L > 0$ sufficiently large so that the no flux boundary condition (14) at $x = L$ does not interact with the traveling wave. The simulations were subject to the following initial conditions:

$$u(x,0) = \begin{cases} 1, & \text{if} \quad x < \alpha, \\ 0 & \text{if} \quad x \geq \alpha, \end{cases} \tag{16}$$
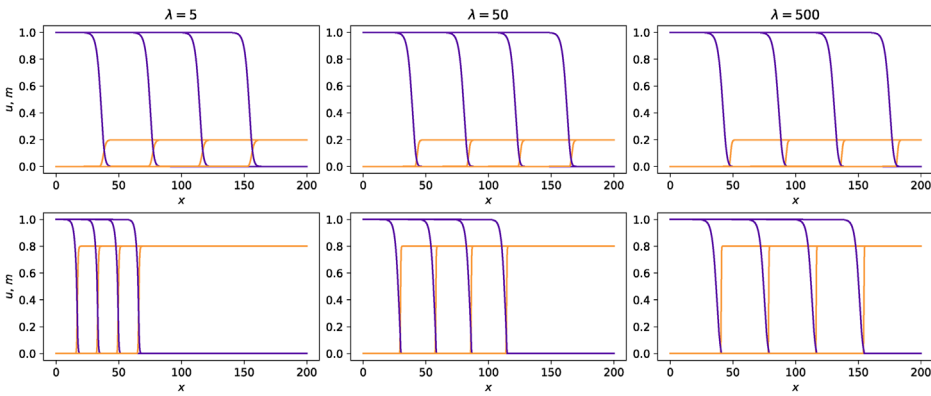
FIGURE 1   Numerical solutions of Equations (12) and (13) subject to the initial conditions (16) and (17), for $m_0 = 0.2$ in the top row and $m_0 = 0.8$ in the bottom row, and for rescaled ECM degradation rates $\lambda = 5, 50, 500$. Cell densities are shown in purple and ECM densities in orange at times $t = 25, 50, 75, 100$ from left to right. Further specifics of the parameter values and the numerical methods used can be found in Appendix B.

$$m(x,0) = \begin{cases} 0, & \text{if} \quad x < \alpha, \\ m_0 & \text{if} \quad x \geq \alpha, \end{cases} \tag{17}$$

where $0 < \alpha \ll L$ represents the width of the initially invaded region at $t = 0$ and $m_0 \in [0,1)$ corresponds to the uninvaded density of ECM ahead of the cells.

We note that, by design, the model (12) and (13) does not permit traveling waves when there are initial conditions with compactly supported cell density and $m_0 = 1$. This is because cells require space ahead of the wave in order to invade; in any regions initially devoid of cells, the ECM cannot be degraded to allow cells to invade. As such, we proceed by considering $m_0 \in [0,1)$. Further specifics of the parameter values and the numerical methods used in this paper can be found in Appendix B.

As shown in Figure 1, when $m_0 \in [0,1)$ the solutions to Equations (12) and (13) subject to the initial conditions (16) and (17) converge to traveling waves whereby the cell density, u, decreases monotonically from one to zero and the ECM density, m, increases monotonically from zero to m_0. The numerical results in Figure 1 also indicate that the speed of the traveling waves changes as the values of the parameters λ and m_0 are changed. This is illustrated in more detail in Figure 2 that also shows that (in agreement with the analytical results presented in Section 3) when $m_0 \in (0,1)$: if $\lambda \to 0^+$ then the speed of the traveling waves converges to $c = 2(1 - m_0)$; whereas if $\lambda \to \infty$ then the speed of the traveling waves converges to $c = 2$.

We also note that when $m_0 = 0$, the solutions to Equation (13) subject to the initial condition (17) are such that $m(x,t) \equiv 0$ for all $t \geq 0$ and thus the model simplifies to the FKPP model (11) with $\hat{D} = \hat{r} = \hat{K} = 1$, that is,

$$\frac{\partial u}{\partial t} = \frac{\partial^2 u}{\partial x^2} + u(1 - u). \tag{18}$$

Consistent with this, numerical simulations indicate that when $m_0 = 0$, the cell density u converges to a traveling wave that decreases monotonically from one to zero (results not shown), and travels with speed $c = 2$ (i.e., the minimal speed of traveling wave solutions to the FKPP model (18)) (see Figure 2).
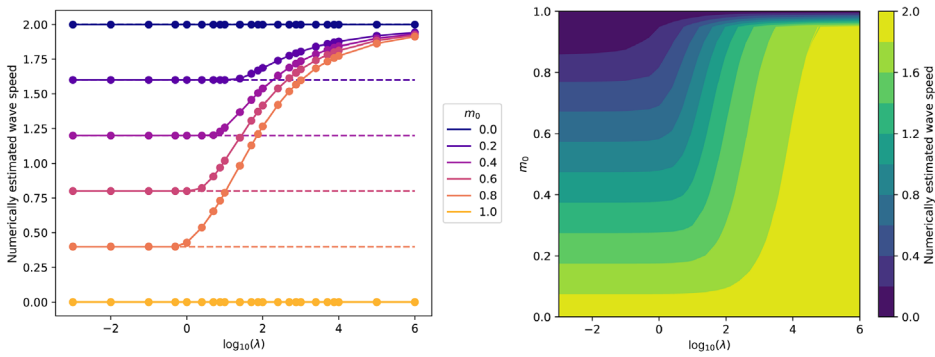
FIGURE 2 The relationship between the numerically estimated speed (solid lines) of traveling wave solutions of Equations (12) and (13) subject to the initial conditions (16) and (17). The dashed lines in the plot on the left highlight the value of $2(1 - m_0)$. The numerically estimated traveling wave speed is obtained by tracing the point $X(t)$ such that $u(X(t), t) = 0.1$. Further specifics of the parameter values and the numerical methods used can be found in Appendix B.

The numerical results summarized in Figure 2 for $m_0 \in [0, 1)$ show similar behaviors to that in El-Hachem et al.,[14] where no volume-filling effects of cells prevent cell movement, while a marked difference is observed for the case $m_0 = 1$, as discussed in Appendix A.

3 | TRAVELING WAVE ANALYSIS

We seek traveling wave solutions of Equations (12) and (13) by adopting the usual traveling wave ansatz $u(x, t) = U(z)$ and $m(x, t) = M(z)$, where $z = x - ct$ with $c > 0$. Since numerical simulations indicate that, for our chosen initial conditions, traveling waves do not emerge when $m_0 = 1$ (see Appendix A), we proceed with this study by exclusively considering the case where $m_0 \in [0, 1)$ that gives

$$\frac{d}{dz}\left[(1 - M)\frac{dU}{dz} + U\frac{dM}{dz}\right] + c\frac{dU}{dz} + U(1 - U - M) = 0, \tag{19}$$

$$c\frac{dM}{dz} - \lambda MU = 0, \tag{20}$$

for $-\infty < z < \infty$ with boundary conditions

$$U(z) \to 1 \quad \text{as} \quad z \to -\infty, \tag{21}$$

$$U(z) \to 0 \quad \text{as} \quad z \to \infty, \tag{22}$$

$$M(z) \to m_0 \quad \text{as} \quad z \to \infty. \tag{23}$$

By expanding Equation (19) and using Equation (20) to substitute in d^2M/dz^2, we find that

$$(1 - M)\frac{d^2U}{dz^2} + c\frac{dU}{dz} + U[(1 - M) - U] = -M\left[U\left(\frac{\lambda U}{c}\right)^2 + \frac{dU}{dz}\left(\frac{\lambda U}{c}\right)\right]. \tag{24}$$

Equation (20), subject to the boundary condition (23), has a semiexplicit solution. That is, if $U(z)$ is known, then we can evaluate $M(z)$ as

$$M(z) = m_0 \exp \left\{ -\frac{\lambda}{c} \int_z^\infty U(s) ds \right\}, \tag{25}$$

which gives

$$M(z) \to 0 \quad \text{as} \quad z \to -\infty, \tag{26}$$

and $M \leq m_0$ for all $z \in \mathbb{R}$. Under the boundary condition $U(z) \to 0$ as $z \to \infty$, at the leading edge of the traveling front (i.e., for $z \in (\ell, \infty)$ with $1 \ll \ell < \infty$ sufficiently large), we can use the ansatz

$$U(z) \approx \exp\{-\alpha z\}, \tag{27}$$

with $0 < \alpha < \infty$ for $z \in (\ell, \infty)$. Inserting Equation (27) into Equation (25) we find

$$M(z) \approx m_0 \exp \left\{ -\frac{1}{\alpha} \left(\frac{\lambda U(z)}{c} \right) \right\}, \tag{28}$$

for $z \in (\ell, \infty)$. Moreover, writing $dU/dz = V$, we can rewrite Equations (19) and (20) as a system of three first-order ordinary differential equations

$$\frac{dU}{dz} = V, \tag{29}$$

$$\frac{dV}{dz} = \frac{1}{(1-M)} \left[-cV - \frac{\lambda}{c} MUV - \frac{\lambda^2}{c^2} MU^3 - U(1 - U - M) \right], \tag{30}$$

$$\frac{dM}{dz} = \frac{\lambda}{c} MU, \tag{31}$$

with boundary conditions given by

$$U(z) \to 1, \quad V(z) \to 0 \quad \text{and} \quad M(z) \to 0 \quad \text{as} \quad z \to -\infty, \tag{32}$$

$$U(z) \to 0, \quad V(z) \to 0 \quad \text{and} \quad M(z) \to m_0 \quad \text{as} \quad z \to \infty. \tag{33}$$

The steady states of the system (29) and (31) with boundary conditions (32) and (33) are given by $S_1 = (1, 0, 0)$ and $S_2 = (0, 0, m_0)$. Traveling wave analysis based on standard linear stability techniques (i.e., standard traveling wave analysis)[30] seeks trajectories in the phase space that connect S_1 at $z = -\infty$ to S_2 at $z = \infty$.[31,32] The eigenvalues of the linearized system at $(U, V, M) = (1, 0, 0)$ are

$$\sigma_1 = \frac{\lambda}{c}, \quad \sigma_{2,3} = \frac{-c \pm \sqrt{c^2 + 4}}{2}, \tag{34}$$

which implies that $(1,0,0)$ is a three-dimensional, hyperbolic, unstable saddle point,[33] which has eigenvectors given by

$$\mathbf{v_1} = \left(\frac{c^2 - \lambda^2}{c^2(\lambda - 1) + \lambda^2}, \quad \frac{\lambda(c^2 - \lambda^2)}{c(c^2(\lambda - 1) + \lambda^2)}, \quad 1 \right)^T, \tag{35}$$
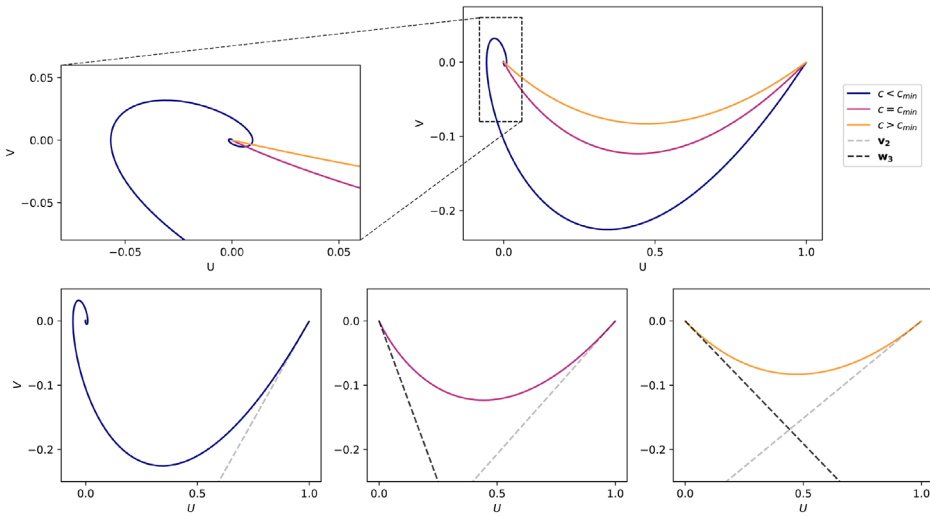
FIGURE 3 Phase plane plot of the system of ordinary differential equations (29) and (30), for different traveling wave speeds, c, demonstrating the change from a stable spiral to a stable node as the traveling wave speed exceeds c_{min}. The corresponding unstable eigenvector given by Equation (36) and stable eigenvector given by Equation (39) are overlaid in the lower plots.[30] Further specifics of the parameter values and the numerical methods used can be found in Appendix B.

$$\mathbf{v}_{2,3} = \left(\frac{c \pm \sqrt{c^2 + 4}}{2}, \quad 0, \quad 1 \right)^T. \tag{36}$$

The eigenvalues of the linearized system at $(U, V, M) = (0, 0, m_0)$ are

$$\sigma_1 = 0, \quad \sigma_{2,3} = \frac{-c \pm \sqrt{c^2 - 4(1 - m_0)^2}}{2(1 - m_0)}, \tag{37}$$

with corresponding eigenvectors

$$\mathbf{w}_1 = (0, 0, 1)^T, \tag{38}$$

$$\mathbf{w}_{2,3} = \left(\frac{c(c \pm \sqrt{c^2 - 4(1 - m_0)^2})}{2\lambda m_0 (m_0 - 1)}, \quad \frac{c(c^2 \pm c\sqrt{c^2 - 4(1 - m_0)^2} - 2(1 - m_0)^2)}{2\lambda m_0 (1 - m_0)^2}, \quad 1 \right)^T, \tag{39}$$

which implies that $(0, 0, m_0)$ is a stable, nonhyperbolic fixed point[34] (see Appendix D for the full derivation). In all cases, we use index 2 to refer to the positive of the two choices and 3 for the negative. When $c^2 - 4(1 - m_0)^2 \leq 0$, the steady-state $(0, 0, m_0)$ is a stable spiral as the eigenvalues have nonzero imaginary parts; however, when $c^2 - 4(1 - m_0)^2 \geq 0$, the steady state is a stable node. In the case that the state $(0, 0, m_0)$ is a stable spiral, U oscillates around this point on its approach and can therefore take negative values (see Figure 3). However, when $(0, 0, m_0)$ is a stable node, there must exist a trajectory from $(1, 0, 0)$ to $(0, 0, m_0)$ contained entirely in the region of phase space defined by $U \geq 0$, $V \leq 0$, and $M \geq 0$, which ensures nonnegativity of U and M, as required to be biologically consistent. This demonstrates the existence of a minimum wave speed, $c_{min} = 2(1 - m_0)$, such that the dependent variables, U and M, remain nonnegative for all

time. It is important to note that $c_{\min}$ is a lower bound on the traveling wave speed, which is only actually attained for this system when the rescaled ECM degradation rate is sufficiently small, that is, $\lambda \to 0^+$ (see Section 3.1). This is clearly shown in Figure 2, which also demonstrates that decreasing m_0 results in an increase in the traveling wave speed.

Traveling wave analysis has also been performed on a PDE model for melanoma invasion into the skin,[35] where volume-filling effects of cells are not considered to impact cell movement,[14] as described earlier. Since traveling wave analysis is always performed on the linearized system, it follows that the additional term describing cell movement prevented by the presence of other cells is lost from Equation (30) during linearization and the minimum traveling wave speed is the same as that derived in El-Hachem et al.[14]: $c_{\min} = 2(1 - m_0)$. Another minimal model for tumor growth was proposed in Colson et al.,[15] where the volume-filling effects of cells were not accounted for in describing cell movement or cell proliferation. Both of these models have the same equation for ECM density as Equation (13), and the models in Refs. [14, 15] have the same flux terms in the equation for cell density evolution, but the model in Colson et al.[15] has one less reaction term since proliferation is unimpeded by the local ECM density. As a result of the fact that all volume-filling effects are encoded in nonlinear terms, changes to the flux terms alone (within this suite of models) have no effect on the predicted minimum traveling wave speed, as they are all identical after linearization. However, alterations to the net proliferation terms do significantly impact the minimum traveling wave speeds predicted by standard traveling wave analysis. Further information regarding these models and their differences can be found in Appendix C.

As previously described, we are particularly interested in investigating the dependence of traveling wave solutions on the parameters λ, the rescaled ECM degradation rate, and m_0, the density of ECM far ahead of the wave. Having now determined that the minimum traveling wave speed decreases linearly as m_0 increases, we now aim to explore the relationship between the numerically estimated traveling wave speed and λ.

Since the traveling wave speed depends on λ, standard perturbation techniques are difficult to apply to the traveling wave equations (19) and (20). As a result, we examine Figure 2 for clues as to how to proceed. We immediately see that for sufficiently small λ it appears that the numerically estimated traveling wave speed is independent of λ and matches the speed predicted by standard traveling wave analysis. It can also be seen from the contour plot in Figure 2 that for large values of λ, the speed converges for all values of $m_0 \in [0, 1)$. As such, we now investigate the asymptotic limits corresponding to slow and fast rescaled ECM degradation rates, $\lambda \to 0^+$ and $\lambda \to \infty$, respectively.

3.1 | Formal asymptotic analysis for $\lambda \to 0^+$

Using Equation (28), it is clear that

$$M(z) \approx m_0 \exp\left\{ -\frac{1}{\alpha}\left(\frac{\lambda\, U(z)}{c} \right) \right\} \to m_0 \quad \text{as} \quad \lambda \to 0^+, \tag{40}$$

for $z \in (\ell, \infty)$ (see Figure 4 or Figures E1 and E2 for the traveling wave profiles).

In the asymptotic regime $\lambda \to 0^+$, substituting Equation (40) into Equation (24) and using the fact that, since $0 \le U(z) < 1$ for $z \in (\ell, \infty)$ and $dU(z)/dz \approx -\alpha\, U(z)$ for $z \in (\ell, \infty)$ (cf. the ansatz
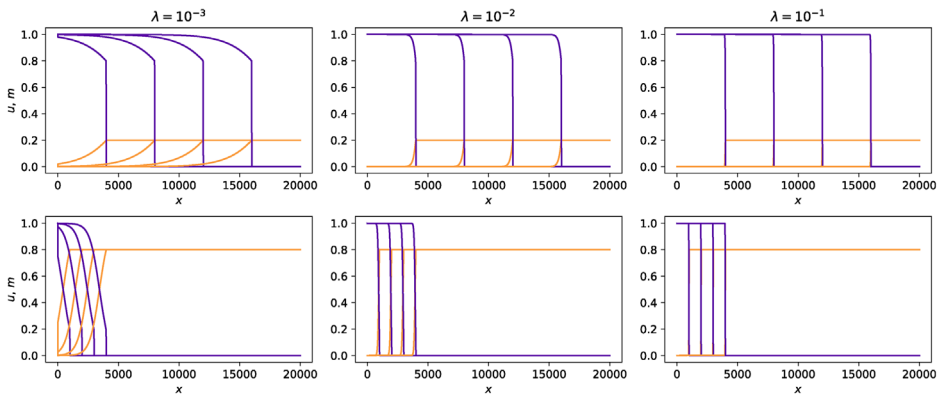
FIGURE 4 Numerical solutions of Equations (12) and (13) subject to the initial conditions (16) and (17), for $m_0 = 0.2$ in the top row and $m_0 = 0.8$ in the bottom row, and for rescaled ECM degradation rates $\lambda = 10^{-3}, 10^{-2}, 10^{-1}$. Cell densities are shown in purple and ECM densities in orange at times $t = 2500, 5000, 7500, 10000$ from left to right. Further specifics of the parameter values and the numerical methods used can be found in Appendix B.

given by Equation (27)), the following asymptotic relation holds:

$$m_0 \exp\left\{ -\frac{1}{\alpha}\left(\frac{\lambda\, U(z)}{c} \right) \right\} \left[U(z)\left(\frac{\lambda\, U(z)}{c} \right)^2 + \frac{dU(z)}{dz}\left(\frac{\lambda\, U(z)}{c} \right) \right] \to 0 \quad \text{as} \quad \lambda \to 0^+, \quad (41)$$

for $z \in (\ell, \infty)$, we find

$$(1 - m_0)\frac{d^2 U(z)}{dz^2} + c\frac{dU(z)}{dz} + U(z)[(1 - m_0) - U(z)] \approx 0, \quad (42)$$

for $z \in (\ell, \infty)$.

Equation (42) is equivalent to the FKPP model (11) in traveling wave coordinates

$$\hat{D}\frac{d^2\hat{U}}{dz^2} + \hat{c}\frac{d\hat{U}}{dz} + \hat{r}\hat{U}\left(1 - \frac{\hat{U}}{\hat{K}} \right) = 0, \quad (43)$$

with $\hat{D} = \hat{r} = \hat{K} = 1 - m_0$, with $\hat{c}_{\min} = 2(1 - m_0)$, as predicted earlier. An excellent match around the leading edge of the traveling wavefront between the traveling wave solution to the FKPP model (11) (Equation (43) in traveling wave coordinates) and Equations (12) and (13) for low values of the rescaled ECM degradation rate can be seen in the plot on the left in Figure 6 (see also Figure 4 or Figures E1 and E2).

We now consider the region $z \in (-\infty, \ell)$ by rescaling Equations (19) and (20) using the new variable $\epsilon = z\lambda$ for $\epsilon \in (-\infty, \ell\lambda]$. The system of Equations (19) and (20) becomes

$$-c\lambda\frac{dU}{d\epsilon} = \lambda^2 \frac{d}{d\epsilon}\left[(1 - M)\frac{dU}{d\epsilon} + U\frac{dM}{d\epsilon} \right] + U(1 - U - M), \quad (44)$$

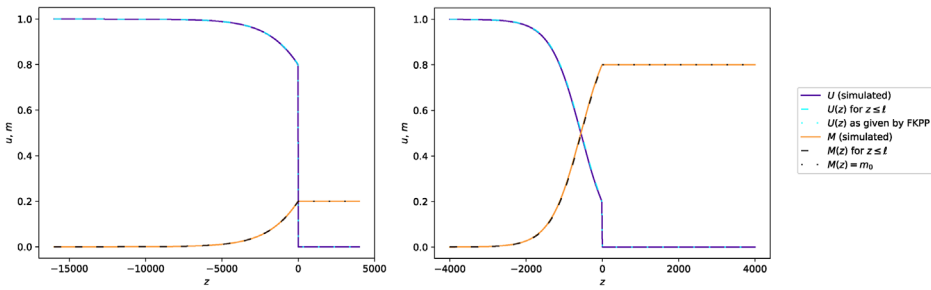$$\lambda\frac{dM}{d\epsilon} = \frac{\lambda}{c}MU. \quad (45)$$

FIGURE 5 Numerical solutions of Equations (12) and (13) subject to the initial conditions (16) and (17), for $m_0 = 0.2$ on the left and $m_0 = 0.8$ on the right with rescaled ECM degradation rate $\lambda = 10^{-3}$ translated into the traveling wave coordinate, z. Solid lines represent the cell and ECM densities from numerical simulations in purple and orange, respectively. The FKPP solution (42) in traveling wave coordinates is plotted as a dotted blue line. The solution $M(z) = m_0$ is plotted in dotted black, and the analytical solutions given by Equations (48) and (49) are plotted in dashed blue and black lines, respectively. Further specifics of the parameter values and the numerical methods used can be found in Appendix B.
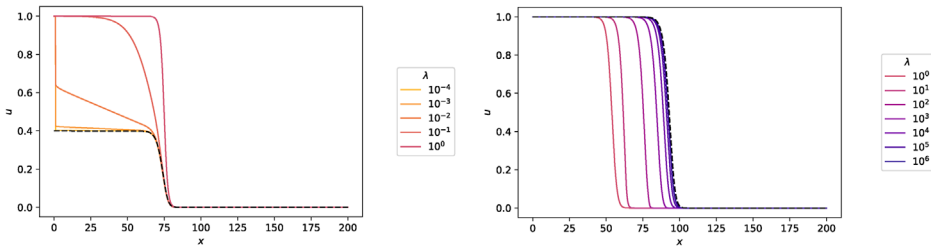

FIGURE 6 Left: plot of the cell density, u, obtained through numerical simulations of Equations (12) and (13) subject to the initial conditions (16) and (17) (solid lines) for small values of λ, and numerical simulations of the FKPP model (11) with rescaled coefficients $\hat{D} = \hat{r} = \hat{K} = 1 - m_0$ (dashed black line) with $t = 100$ and $m_0 = 0.6$. Right: plot of the cell density, u, obtained through numerical simulations of Equations (12) and (13) subject to the initial conditions (16) and (17) (solid lines) for large values of λ, and numerical simulations of the FKPP model (18) (dashed black line) in the plot on the right for $t = 50$ and $m_0 = 0.4$. Qualitatively, the same behavior is observed for all $m_0 \in [0, 1)$. Further specifics of the parameter values and the numerical methods used for the simulations can be found in Appendix B.

For $\lambda \to 0^+$, we find from Equation (44) that $U(\epsilon)(1 - U(\epsilon) - M(\epsilon)) = 0$, so that for $\epsilon \in (-\infty, \ell\lambda]$ we have $U(\epsilon) = 1 - M(\epsilon)$ since $U(\epsilon) \to 1$ as $\epsilon \to -\infty$. By substitution into Equation (45), we find

$$\frac{dM}{d\epsilon} = \frac{M(1 - M)}{c},$$

which, using the matching condition that $M(\epsilon = \ell\lambda) = m_0$, gives

$$M(\epsilon) = \frac{m_0 \exp\{-(\lambda\ell - \epsilon)/c\}}{1 - m_0 + m_0 \exp\{-(\lambda\ell - \epsilon)/c\}}, \tag{46}$$

Recalling that $U(\epsilon) = 1 - M(\epsilon)$, we obtain

$$U(\epsilon) = \frac{1 - m_0}{1 - m_0 + m_0 \exp\{-(\lambda\ell - \epsilon)/c\}}, \tag{47}$$

which tends to 1 as $\epsilon \to -\infty$ and to $1 - m_0$ as $\epsilon \to \ell\lambda$. In the traveling wave coordinate, z, Equation (47) can be written as

$$U(z) = \frac{1 - m_0}{1 - m_0 + m_0 \exp\{-\lambda(\ell - z)/c\}}, \tag{48}$$

for $z \in (-\infty, \ell]$ and the solution to the FKPP model, as given by Equation (42), for $z \in (\ell, \infty)$. In the traveling wave coordinate, z, the solution for the wave profile of the ECM given by Equation (46) is

$$M(z) = \frac{m_0 \exp\{-\lambda(\ell - z)/c\}}{1 - m_0 + m_0 \exp\{-\lambda(\ell - z)/c\}}, \tag{49}$$

for $z \in (-\infty, \ell]$, and $M(z) = m_0$ for $z \in (\ell, \infty)$, as given by Equation (40). An excellent agreement between these analytical solutions and the numerical results can be observed in Figure 5.

Similar models, such as those described at the end of Section 3 that do not have volume-filling effects taken into account, demonstrate qualitatively similar behavior. In all of these models, at very low rescaled ECM degradation rates we observe convergence of the solutions to those of the FKPP model with rescaled parameters. For models with the same cell proliferation term as in Equation (12), the rescaled parameters are the same and the convergence has qualitatively similar behavior, as displayed in the plot on the left in Figure 6. As a result, in the limit of very small rescaled ECM degradation rates, $\lambda \to 0^+$, the model (12) and (13) can be simplified to that presented in El-Hachem et al.,[14] which neglects the volume-filling effects of cells upon cell movement. This model can, in turn, be well approximated by the FKPP model (11) with rescaled parameters $\hat{D} = \hat{r} = \hat{K} = 1 - m_0$. This result is consistent with predictions from standard traveling wave analysis. However, for the model presented in Colson et al.,[15] the parameters of the rescaled FKPP model to which the model converges are, instead, $\hat{D} = 1 - m_0$ and $\hat{r} = \hat{K} = 1$, that entails a higher cell carrying capacity density since proliferation is not impacted by the surrounding ECM. (See Appendix C for a more detailed comparison.) As such, the model (12) and (13) is poorly approximated using models, such as that in Colson et al.,[15] with different underlying assumptions for cell proliferation. These differences highlight the importance of fully laying out all of the model assumptions at the single-cell level before deriving the PDE model, so that the population-level model fully captures behaviors associated with the underlying cell-level assumptions, in all parameter regimes.

3.2 | Formal asymptotic analysis for $\lambda \to \infty$

In the case of very large rates of ECM degradation, by considering the semiexplicit solution for M in terms of U given by Equation (28), we see that

$$M(z) \approx m_0 \exp\left\{-\frac{1}{\alpha}\left(\frac{\lambda U(z)}{c}\right)\right\} \to 0 \quad \text{as} \quad \lambda \to \infty, \tag{50}$$

for $z \in (\ell, \infty)$ (see Figure 7 or Figure E3 for the traveling wave profiles). In the asymptotic regime $\lambda \to \infty$, substituting Equation (50) into Equation (24) and using the fact that, since $0 \le U(z) < 1$ for $z \in (\ell, \infty)$ and $dU(z)/dz \approx -\alpha U(z)$ for $z \in (\ell, \infty)$ (cf. the ansatz given by Equation (27)), the
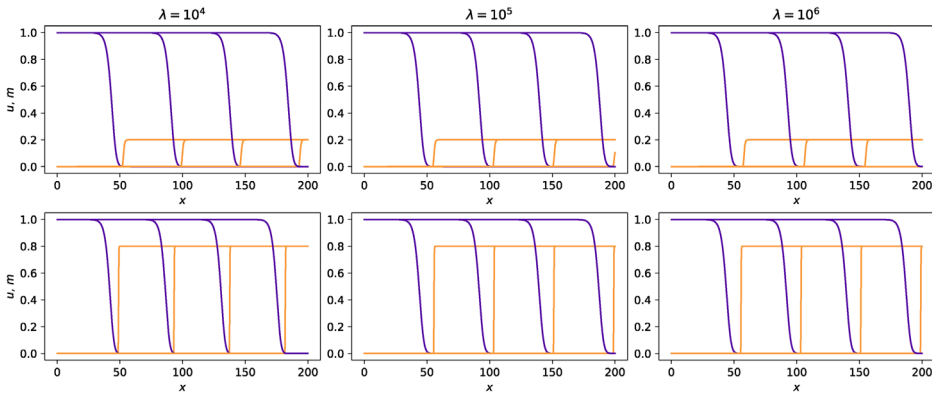
FIGURE 7 Numerical solutions of Equations (12) and (13) subject to the initial conditions (16) and (17), for $m_0 = 0.2$ in the top row and $m_0 = 0.8$ in the bottom row, and for rescaled ECM degradation rates $\lambda = 10^4, 10^5, 10^6$. Cell densities are shown in purple and ECM densities in orange at times $t = 25, 50, 75, 100$ from left to right. Further specifics of the parameter values and the numerical methods used can be found in Appendix B.

following asymptotic relation holds:

$$m_0 \exp\left\{-\frac{1}{\alpha}\left(\frac{\lambda U(z)}{c}\right)\right\}\left[U(z)\left(\frac{\lambda U(z)}{c}\right)^2 + \frac{dU(z)}{dz}\left(\frac{\lambda U(z)}{c}\right)\right] \to 0 \quad \text{as} \quad \lambda \to \infty, \quad (51)$$

for $z \in (\ell, \infty)$, we find

$$\frac{d^2 U(z)}{dz^2} + c\frac{dU(z)}{dz} + U(z)(1 - U(z)) \approx 0, \quad (52)$$

for $z \in (\ell, \infty)$. Hence, when $\lambda \to \infty$ we expect $U(z)$ at the leading edge of the traveling front to behave, to a first approximation, as the solution to the FKPP equation (18) in traveling wave coordinates subject to the boundary condition (22), for which $c_{\min} = 2$. This result can also be observed numerically in the plot on the right of Figure 6. The same behavior is observed in similar models without volume-filling effects,[14,15] demonstrating that the model (12) and (13) can be approximated, to an extent, with any of these simpler models in the parameter regime $\lambda \to \infty$, as growth and diffusion are unrestricted by the ECM within a neighborhood of the traveling wavefront.

4 | DISCUSSION AND CONCLUSIONS

In this paper, a model for cell invasion into the surrounding ECM has been studied by considering primarily its traveling wave solutions. In this model, derived from the first principles from an agent-based model describing cell-level behaviors, cells evolve under the action of diffusion and proliferation, that is coupled to degradation of the surrounding ECM. As a result of volume-fillling effects, cells require space ahead of the wavefront in order to invade the domain.

Numerical solutions of the PDE model (12) and (13) demonstrate a complex relationship between the traveling wave speed, c, the density of ECM far ahead of the wave of cells, m_0, and the rescaled ECM degradation rate, λ. Partial relationships between these parameters in asymptotic regimes of interest have been established, including that $c \to 2(1 - m_0)$ as $\lambda \to 0^+$ and that

TABLE 1 Description of the volume-filling effects of cells and ECM considered by the models compared in this study.

Model	Volume-filling in movement		Diffusion term	Volume-filling in proliferation		Reaction term
	By cells	By ECM		By cells	By ECM	
Colson[15]	−	+	$\frac{\partial}{\partial x}[(1-m)\frac{\partial u}{\partial x}]$	+	−	$u(1-u)$
Browning[14,35]	−	+	$\frac{\partial}{\partial x}[(1-m)\frac{\partial u}{\partial x}]$	+	+	$u(1-u-m)$
Equations (12) and (13)	+	+	$\frac{\partial}{\partial x}[(1-m)\frac{\partial u}{\partial x} + u\frac{\partial m}{\partial x}]$	+	+	$u(1-u-m)$

Abbreviation: ECM, extracellular matrix.

$c \to 2^-$ as $\lambda \to \infty$. A good agreement with the FKPP model (11) has been demonstrated in the case where $\lambda \to \infty$, and we showed that the impacts of introducing volume-filling effects of cells to reduce cell movement (in comparison to the model in El-Hachem et al.[14]) are minimal. As such, the FKPP model (11) provides a suitable model simplification to reproduce the qualitative behaviors of the fully dimensional system in the case of a large ECM degradation rate, $\tilde{\lambda}$, compared to the proliferation rate, $\tilde{r}$. Since $\lambda = \tilde{\lambda}\tilde{K}/\tilde{r}$, the results equivalently suggest that as $\tilde{K} \to \infty$, the system can be well modeled by the FKPP model (11). This describes a model where volume-filling effects are negligible, and thus the speed of the invasion front is given by $c_{\min} = 2$. For $\lambda \to 0^+$, which is representative of very large proliferation rates compared to the rescaled ECM degradation rates, or extremely small carrying capacities, the system can be studied by considering the simplification to a rescaled FKPP model (42). In this case, traveling waves are observed for $m \in [0, 1)$, but the speed of the invasion front is now given by $c_{\min} = 2(1 - m_0)$. Converting back to dimensional variables, as with the FKPP model (11), the analytically predicted traveling wave speed increases with the cell proliferation rate, but with a more complicated relationship for the regions of parameter space corresponding to where the relationship between the traveling wave speed and rescaled ECM degradation rate is not yet well established. It is likely this complicated relationship indicates that the system exhibits changes between pulled, pushed, and semipushed waves due to the nonlinear cross-species dynamics that vary in strength for different parameter values.[36] This could be investigated further by examining the ratio between the traveling wave speeds for different parameter values.

It is also clear that qualitatively similar results are observed between this new model with volume-filling, and previously studied models outside this framework, as described by Table 1, in all cases where $m_0 \in [0, 1)$. Therefore, it could be said that the model originally proposed in Browning et al.[35] provides a good model simplification for any case where $m_0 \in [0, 1)$. In the case where $m_0 = 1$, the region that is initially uninvaded by cells is full of ECM, such that proliferation and movement of cells into this region is entirely prevented. This result provides the starkest difference between the model studied in this paper and those previously studied elsewhere.[14,15] It is observed that in the case of compactly supported initial cell density, cell invasion cannot occur into the region where $m(x, 0) = 1$, $u(x, 0) = 0$, and thus pinning occurs and traveling waves cannot form.[37] It is biologically reasonable to assume that an invading cell population might have zero density far ahead of the invading front. However it is important to note that the model considered here is a very simplistic model for cell invasion into ECM, and if further biological complications, such as the secretion of matrix metalloproteinases (MMPs) by cells to degrade and remodel ECM, were introduced then these phenomenological results would no longer be observed.[38] This

is because we could reasonably assume MMPs could still diffuse into regions occupied entirely by ECM, and then degrade it.

The overall conclusion of our study is that there exist simpler models for cell invasion into ECM such as Refs. [6, 14, 15] that are defined by similar guiding principles and can be used to reproduce the qualitative behaviors of the traveling waves observed in the model presented in this work. Analysis of these systems confirms that the qualitative model predictions are conserved, and therefore the simpler models can be used in future studies to reduce computational complexity and make the resulting PDE model more analytically tractable. The disadvantage of this conclusion, however, is that in order to use these models to infer parameters from data, extra steps would be required to validate whether the correct model has been selected. For example, analysis of cell trajectories can help infer the cell–cell interactions underlying the motility mechanism and distinguish between the suite of models with qualitatively similar behaviors.[39–41] Our results reveal that the reaction term significantly impacts the traveling wave speed for small and intermediate values of λ and thus it could be used to inform model development, by defining the reaction term by considering whether space or nutrients are the limiting factor for cell invasion into ECM; and model selection, by comparing the expected wave speeds to the data.

There are a variety of possible extensions to the work presented in this paper. The underlying on-lattice agent-based model of cell movement involves a number of simplifying assumptions, such as that cells can only degrade ECM agents in the same lattice site. By varying these assumptions, there would be the possibility to expand the biological applicability of the study to determine under which regimes the resulting models can also be approximated by simpler seminal models of cell invasion. Different proliferation terms, as well as terms to account for ECM evolution in more detail could be included, such as ECM remodeling by cells, or elastic deformation.[42] Beyond this, another clear extension of this work would be to introduce further spatial dimensions, or different geometries, that are particularly interesting for studying cancer cell invasion, and to investigate the stability of the traveling wave solutions for the different possible models. For the case $\lambda \to 0^+$, there is an opportunity to apply boundary layer theory and asymptotic analysis to arrive at an expression for the full traveling wave profile at long times. It would also be of particular interest to arrive at some functional form for the traveling wave speed, $c(\lambda, m_0)$, for all possible parameter values and to define the critical value of λ_c, depending on m_0 (see Figure 2), whereby for $\lambda < \lambda_c$ the minimum traveling wave speed observed numerically matches that predicted by standard traveling wave analysis $c = c_{\min}$. The critical value, λ_c, might be found by establishing the basins of attraction for each steady-state and seeking parameter regimes where the dynamics follow different paths. If possible, this knowledge could then further aid an investigation using perturbation methods into the shape of the wavefront for intermediate values of λ and by characterizing this behavior, this model could be used to describe biological scenarios such as tumor growth, where λ would represent the rate at which the tumor cells were able to degrade ECM in the surrounding environment.

DATA AVAILABILITY STATEMENT

Data sharing is not applicable to this article as no datasets were generated or analyzed during the current study.

ORCID

Rebecca M. Crossley 🄳 https://orcid.org/0000-0001-7342-0207

REFERENCES

1. Giniūnaitė R, Baker RE, Kulesa PM, Maini PK. Modelling collective cell migration: neural crest as a model paradigm. *J Math Biol*. 2020;80:481-504.
2. Johnston ST, Baker RE, McElwain DL, Simpson MJ. Co-operation, competition and crowding: a discrete framework linking Allee kinetics, nonlinear diffusion, shocks and sharp-fronted traveling waves. *Sci Rep*. 2017;7(1):1-19.
3. Dallon JC, Sherratt JA, Maini PK. Mathematical modelling of extracellular matrix dynamics using discrete cells: fiber orientation and tissue regeneration. *J Theor Biol*. 1999;199(4):449-471
4. Perumpanani AJ, Byrne HM. Extracellular matrix concentration exerts selection pressure on invasive cells. *Eur J Cancer*. 1999;35(8):1274-1280.
5. Painter KJ, Sherratt JA. Modelling the movement of interacting cell populations. *J Theor Biol*. 2003;225(3):327-339.
6. Fisher RA. The wave of advance of advantageous genes. *Ann Eugen*. 1937;7(4):355-369.
7. Kolmogorov AN, Petrovskii I, Piskunov NS. A study of the equation of diffusion with increase in the quantity of matter, and its application to a biological problem. *Moscow Univ Biol Sci Bull*. 1937;1(6):1-25.
8. Maini PK, McElwain DLS, Leavesley DI. Traveling wave model to interpret a wound-healing cell migration assay for human peritoneal mesothelial cells. *Tissue Eng*. 2004;10(3-4):475-482.
9. Gerlee P, Nelander S. Travelling wave analysis of a mathematical model of glioblastoma growth. *Math Biosci*. 2016;276:75-81.
10. Okubo A, Maini PK, Williamson MH, Murray JD. On the spatial spread of the grey squirrel in Britain. *Proc R S London. B. Biol Sci*. 1989;238(1291):113-125.
11. Kot M. *Elements of Mathematical Ecology*. Cambridge University Press; 2001.
12. Canosa J. On a nonlinear diffusion equation describing population growth. *IBM J Res Dev*. 1973;17(4):307-313.
13. Murray JD. *Mathematical Biology I: An Introduction*. Springer; 2002.
14. El-Hachem M, McCue SW, Simpson MJ. Travelling wave analysis of cellular invasion into surrounding tissues. *Physica D*. 2021;428:133026.
15. Colson C, Sánchez-Garduño F, Byrne HM, Maini PK, Lorenzi T. Travelling-wave analysis of a model of tumour invasion with degenerate, cross-dependent diffusion. *Proc R Soc A*. 2021;477(2256):20210593.
16. Gurtin ME, MacCamy RC. On the diffusion of biological populations. *Math Biosci*. 1977;33(1-2):35-49.
17. Sengers BG, Please CP, Oreffo ROC. Experimental characterization and computational modelling of two-dimensional cell spreading for skeletal regeneration. *J R Soc Interface*. 2007;4(17):1107-1117.
18. Martin NK, Gaffney EA, Gatenby RA, Maini PK. Tumour–stromal interactions in acid-mediated invasion: a mathematical model. *J Theor Biol*. 2010;267(3):461-470.
19. McGillen JB, Gaffney EA, Martin NK, Maini PK. A general reaction–diffusion model of acidity in cancer invasion. *J Math Biol*. 2014;68(5):1199-1224.
20. Simpson MJ, Hughes BD, Landman KA. Diffusing populations: ghosts or folks? *Australas J Eng Educ*. 2009;15(2):59-68.
21. Simpson MJ, Landman KA, Hughes BD. Multi-species simple exclusion processes. *Physica A*. 2009;388(4):399-406.
22. Anderson ARA, Rejniak KA, Gerlee P, Quaranta V. Microenvironment driven invasion: a multiscale multimodel investigation. *J Math Biol*. 2009;58:579-624.
23. Kim Y, Othmer HG. Hybrid models of cell and tissue dynamics in tumor growth. *Math Biosci Eng*. 2015;12(6):1141.
24. Tam A, Green JEF, Balasuriya S, et al. Nutrient-limited growth with non-linear cell diffusion as a mechanism for floral pattern formation in yeast biofilms. *J Theor Biol*. 2018;448:122-141.

25. Bruna M, Chapman JS. Diffusion of multiple species with excluded-volume effects. *J Chem Phys*. 2012;137(20):204116.

26. Morris B, Curtin L, Hawkins-Daarud A, et al. Identifying the spatial and temporal dynamics of molecularly-distinct glioblastoma sub-populations. *Math Biosci Eng*. 2020;17(5):4905.

27. Painter KJ, Hillen T. Volume-filling and quorum-sensing in models for chemosensitive movement. *Can Appl Math Q*. 2002;10(4):501-543.

28. Taylor PR, Baker RE, Simpson MJ, Yates CA. Coupling volume-excluding compartment-based models of diffusion at different scales: Voronoi and pseudo-compartment approaches. *J R Soc Interface*. 2016;13(120):20160336.

29. Penington CJ, Hughes BD, Landman KA. Building macroscale models from microscale probabilistic models: a general probabilistic approach for nonlinear diffusion and multispecies phenomena. *Phys Rev E*. 2011;84(4):041120.

30. Curtin L, Hawkins-Daarud A, Van Der Zee KG, Swanson KR, Owen MR. Speed switch in glioblastoma growth rate due to enhanced hypoxia-induced migration. *Bull Math Biol*. 2020;82(3):43.

31. Murray JD. *Mathematical Biology II: Spatial Models and Biomedical Applications*. Vol. 3. Springer New York; 2001.

32. Lam K-Y, Lou Y. *Introduction to Reaction-Diffusion Equations: Theory and Applications to Spatial Ecology and Evolutionary Biology*. Springer; 2022.

33. Anton H, Bivens I, Davis S. *Calculus: Multivariable version*. Von Hoffmann Press; 2001.

34. Wiggins S, Golubitsky M. *Introduction to Applied Nonlinear Dynamical Systems and Chaos*. Texts in Applied Mathematics, Vol. 2. Springer; 2003.

35. Browning AP, Haridas P, Simpson MJ. A Bayesian sequential learning framework to parameterise continuum models of melanoma invasion into human skin. *Bull Math Biol*. 2019;81(3):676-698.

36. Birzu G, Hallatschek O, Korolev KS. Fluctuations uncover a distinct class of traveling waves. *Proc Natl Acad Sci*. 2018;115(16):E3645-E3654.

37. Wang C-H, Matin S, George AB, Korolev KS. Pinned, locked, pushed, and pulled traveling waves in structured environments. *Theor Popul Biol*. 2019;127:102-119.

38. Perumpanani AJ, Simmons DL, Gearing AJH, et al. Extracellular matrix-mediated chemotaxis can impede cell migration. *Proc R Soc B: Biol Sci*. 1998;265(1413):2347.

39. Simpson MJ, Landman KA, Hughes BD. Pathlines in exclusion processes. *Phys Rev E*. 2009;79(3):031920.

40. Bowden LG, Simpson MJ, Baker RE. Design and interpretation of cell trajectory assays. *J R Soc Interface*. 2013;10(88):20130630.

41. Ross RJH, Yates CA, Baker RE. Inference of cell–cell interactions from population density characteristics and cell trajectories on static and growing domains. *Math Biosci*. 2015;264:108-118.

42. Malik AA, Wennberg B, Gerlee P. The impact of elastic deformations of the extracellular matrix on cell migration. *Bull Math Biol*. 2020;82:1-19.

43. Strobl MAR, Krause AL, Damaghi M, Gillies R, Anderson ARA, Maini PK. Mix and match: phenotypic coexistence as a key facilitator of cancer invasion. *Bull Math Biol*. 2020;82(1):15.

44. Morton KW, Mayers DF. *Numerical Solution of Partial Differential Equations: An Introduction*. 2nd ed. Cambridge University Press; 2005.

APPENDIX A: MAIN RESULTS OF NUMERICAL SIMULATIONS FOR $m_0 = 1$

As demonstrated in Figure 2, when $m_0 = 1$, the system (12) and (13) subject to the initial conditions (16) and (17) does not permit traveling wave solutions. To investigate this further, we simulate

the system (12) and (13) subject to different initial conditions. In every case, we consider the initial condition for the ECM density, m, given by

$$m(x,0) = \begin{cases} m_0 - u(x,0), & \text{if} \quad m_0 > 1 - \gamma, \\ m_0, & \text{if} \quad m_0 \leq 1 - \gamma, \end{cases} \tag{A1}$$

with $0 \leq \gamma \leq 1$, which depends on the initial cell density, $u(x,0)$. To explore the behaviors observed at $m_0 = 1$, we consider two different options for $u(x,0)$ in this appendix. First, we consider the compactly supported initial condition

$$u(x,0) = \begin{cases} \gamma\left(1 - \tanh\left(\frac{x}{\epsilon}\right)\right), & \text{if} \quad \gamma\left(1 - \tanh\left(\frac{x}{\epsilon}\right)\right) \geq \xi, \\ 0, & \text{if} \quad \gamma\left(1 - \tanh\left(\frac{x}{\epsilon}\right)\right) < \xi, \end{cases} \tag{A2}$$

and alternatively, the following noncompactly supported initial conditions, as used in El-Hachem et al.,[14]

$$u(x,0) = \begin{cases} \gamma, & x < \beta, \\ \gamma \exp\{-a(x-\beta)\}, & x \geq \beta. \end{cases} \tag{A3}$$

Here, $\gamma \in [0,1]$ represents the maximum cell density at $t = 0$ and $m_0 \in [0,1]$ corresponds to the uninvaded density of ECM. Moreover, in the definition given by Equation (A2), the parameter $\xi \in (0,1]$ is used to control the tolerance below which the cell density can be assumed, on a first approximation, to be zero, and $\epsilon > 0$ represents the initial width of the cell density profile. Finally, in the definition given by Equation (A3), the parameter $\beta \in \mathbb{R}$ is used to define a region where the cell density is initially constant and equal to $\gamma \in [0,1]$, while the parameter $a > 0$ is used to prescribe the lengthscale over which the cell density profile decays. We note that, since γ, $m_0 \in [0,1]$, the initial conditions (A1), (A2), and (A3) are such that the total density of cells and ECM at $t = 0$ does not locally exceed the extreme value 1, which corresponds to complete local saturation, that is, $u(x,0) + m(x,0) \leq 1$ for all $x \in [0,L]$. We also note that when $m_0 = 0$ the initial condition (A1) reduces to the trivial initial condition $m(x,0) \equiv 0$.

The numerical results in Figure A1A, which complement the results summarized by Figure 2, show that when $m_0 = 1$ the system (12) and (13) subject to the initial conditions with compactly support cell density (A2) cannot sustain traveling wave solutions. On the other hand, the numerical results in Figure A1B demonstrate that traveling wave solutions can be sustained in the case where noncompactly supported initial conditions (A3) in u are considered.

This result is a consequence of the volume-filling effects of cells. By considering an initial condition where $m(x,0) = 1$ ahead of the invading population, due to volume-filling, the invading population is unable to penetrate the region where $u = 0$, $m = 1$. This agrees with the agent-based description since cells are only able to degrade ECM in the same lattice site.

As such, for the model (12) and (13), whenever $m_0 = 1$ and there are compactly supported initial conditions in u, invasion is entirely prevented beyond a point x^*, that is the smallest x such that $u(x,0) = 0$ for all $x \geq x^*$. This result is starkly different from simpler models in the literature that do not include volume-filling effects of cells and ECM, such as Refs. [14, 15], where the total density of cells and ECM is not bounded above and cells can invade into a region where $u = 0$, $m = 1$, and thus exhibit traveling wave solutions.
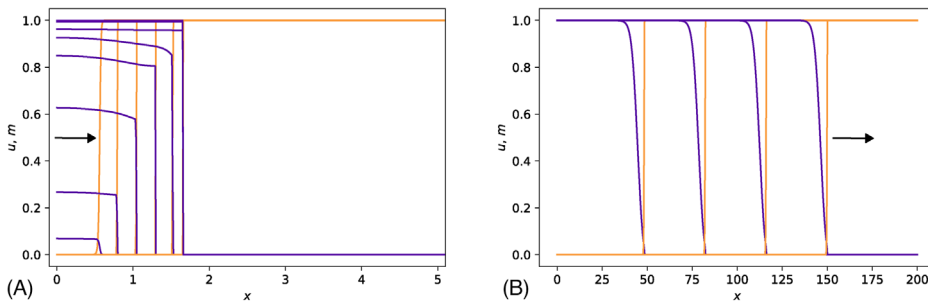
FIGURE A1 Numerical solutions to the system (12) and (13) subject to the initial conditions (A1) and (A2) (panel (A)) or (A1) and (A3) (panel (B)), for $m_0 = 1$ and $\lambda = 250$. Cell densities are shown in purple and ECM densities in orange at times $t = 2, 4, 6, 8, 10, 12, 14, 16$ (from left to right) in panel (A) and times $t = 25, 50, 75, 100$ (from left to right) in panel (B). Note that the axis in the plot in panel (a) is zoomed in on $x \in [0, 5]$ to display the initial behavior in the transient region before invasion stops. Further specifics of the parameter values and the numerical methods used for simulation can be found in Appendix B.

APPENDIX B: NUMERICAL METHODS

Equations (12) and (13) are solved numerically subject to no flux boundary conditions (14) in u at $x = 0$ and $x = L$ using the method of lines on the one-dimensional spatial domain $[0, L]$ where $L > 0$ is chosen to be sufficiently large to remove boundary effects. In most cases, we take $L = 200$. The spatial domain is uniformly discretized with spacing $\Delta = 0.1$ between each of the $i = 1, \ldots, I$ spatial points, and the following discretization is used[43]:

$$\frac{\partial}{\partial x}\left[D\frac{\partial a}{\partial x}\right]_i \approx \frac{1}{2\Delta^2}[(D_{i-1} + D_i)a_{i-1} - (D_{i-1} + 2D_i + D_{i+1})a_i + (D_i + D_{i+1})a_{i+1}], \quad (B1)$$

where a_i represents the value of a at the spatial point i. For the model (12) and (13), we use this discretization twice, with $D = (1 - m)$, $a = u$ and for the second term in the flux as $D = u$, $a = m$. Equations (12) and (13) can then be rewritten as a system of $2I$ ordinary differential equations given by

$$\frac{du_i}{dt} = \frac{1}{2\Delta^2}[u_{i-1}(1 - m_i) + u_i(m_{i+1} + m_{i-1} - 2) + u_{i+1}(1 - m_i)] + u_i(1 - u_i - m_i), \quad (B2)$$

$$\frac{dm_i}{dt} = -\lambda m_i u_i, \quad (B3)$$

for $1 \leq i \leq I - 1$. To implement the boundary conditions, we introduce the ghost points x_{-1} and x_{I+1}[44] and set

$$u_0(t) = u_{-1}(t), \qquad u_{I+1}(t) = u_I(t), \qquad \forall t \geq 0, \quad (B4)$$

so that

$$\frac{du_0}{dt} = 2(u_1 - u_0) + u_0(1 - u_0 - m_0), \quad (B5)$$

$$\frac{du_I}{dt} = 2(u_{I-1} - u_I) + u_I(1 - u_I - m_I). \quad (B6)$$

We solve the system of equations (B2) and (B3) and (B5) and (B6) using the built-in Python solver scipy.integrate.solve_ivp with the explicit Runge–Kutta integration method of order 5 and time step $\tau = 1$. Convergence checks were completed by considering a range of tolerances, time, and spatial steps to ensure that the parameters used for simulations produced solutions within the second-order error associated with the numerical scheme.

For the simulations of the PDE systems in this work, we consider compactly supported initial conditions (16) and (17) with $\alpha = 1$. In Appendix A, we use $\xi = 10^{-7}$, $\gamma = 0.1$, and $\epsilon = 1$ when considering compactly supported initial conditions (A1) and (A2), and $a = 0.1$, $\gamma = 0.1$, and $\beta = 10$ for noncompactly supported initial conditions (A1) and (A3). Varying these parameters reproduces the behaviors observed in El-Hachem et al.[14]

In Figure 3, we show the results of numerically solving Equations (29) and (30) with the initial condition $(U, V, M) = (0.9, -0.01, 0.01)$ for $c = 1$, $2(1 - m_0)$, 3 with time step $\tau = 0.01$ and final time $t = 100$ using Python's built-in stiff solver scipy.integrate.ODE with tolerance 10^{-15} and order 5.

APPENDIX C: COMPARISON TO OTHER MODELS IN THE LITERATURE

This study focuses on the impact of introducing volume-filling effects of cells and ECM to a model of cell invasion into ECM. There are a number of PDE model simplifications in the literature, including the following model, proposed as a minimal model for tumor growth into ECM in Colson et al.[15]:

$$\frac{\partial u}{\partial t} = \frac{\partial}{\partial x}\left[(1 - m)\frac{\partial u}{\partial x}\right] + u(1 - u), \tag{C1}$$

$$\frac{\partial m}{\partial t} = -\lambda mu, \tag{C2}$$

that assumes cell motility to be impacted by the presence of surrounding ECM only and cell proliferation impacted only by other cells, that is, the resource limiting cell proliferation is not space. Another similar model is presented in Browning et al.[35] to describe melanoma growth into skin and it is subsequently analyzed in El-Hachem et al.[14] The model can be interpreted to assume that cell motility is decreased by ECM and that cell proliferation is impacted by both other cells and ECM:

$$\frac{\partial u}{\partial t} = \frac{\partial}{\partial x}\left[(1 - m)\frac{\partial u}{\partial x}\right] + u(1 - u - m), \tag{C3}$$

$$\frac{\partial m}{\partial t} = -\lambda mu. \tag{C4}$$

The model variables and parameters are interpreted in the same way as in the model presented in this work (12) and (13).

We are particularly interested in comparing the population-level behaviors of the PDE model for cell invasion into ECM presented in this work, which incorporates volume-filling effects into both diffusion and proliferation of cells, to the simpler models without these volume-filling effects, presented in the literature. By looking at Figure C1, we can draw the following conclusions: all three models produce traveling wave solutions with a speed $c \geq c_{\min}$, where $c_{\min}$ is the minimum speed predicted by standard traveling wave analysis. In fact, all of these speeds are dependent on both the initial density of ECM ahead of the wave, m_0, and the rescaled ECM degradation rate λ. The two models with the same reaction (growth) terms, depending on both cell and
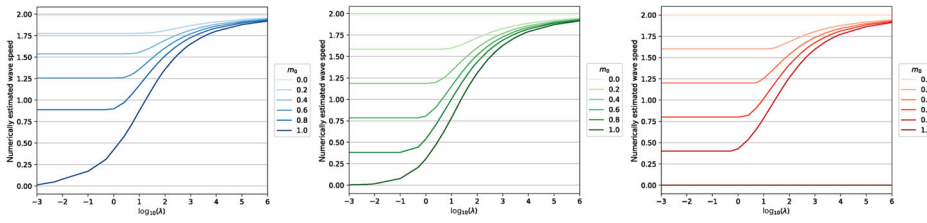
FIGURE C1 The relationship between the numerically estimated speed of traveling wave solutions to the system (C1) and (C2) on the left (blue), (C3) and (C4) in the middle (green), and (12) and (13) on the right (red), subject to the initial conditions (16) and (17). The numerically estimated traveling wave speed is obtained by tracing the point $X(t)$ such that $u(X(t), t) = 0.1$. Further specifics of the parameter values and the numerical methods used can be found in Appendix B.

ECM preventing growth, predict the same traveling wave speed $c_{\min} = 2(1 - m_0)$, that is achieved numerically for $\lambda \to 0^+$. However, the model (C1) and (C2) presented in Colson et al.[15] predicts a speed $c_{\min} = 2\sqrt{1 - m_0}$, that is also revealed for $\lambda \to 0^+$. As a result, the behaviors observed in these models for small rescaled ECM degradation rates λ can be reproduced by studying a FKPP model (11) with the appropriate parameters. In the same manner, by looking at Figure C1, it is clear that all three models produce traveling waves with speed $c \to 2^-$ as $\lambda \to \infty$. The behaviors observed here can be studied by considering the standard FKPP model (18) with all parameters equal to unity. The FKPP model (18) is also a suitable model simplification for all three systems when $m_0 = 0$.

The transition between the two asymptotic regions is yet to be fully characterized for any of the models, but it is clear that c is a monotonic, increasing function of λ and m_0 for all of the models. The critical value above which λ begins to influence the speed is similar across the models but clearly depends on m_0 and takes larger values across the models as more volume-filling effects are taken into account. Following intuition, we also find that, in general, the speed of invasion is slower as volume-filling effects are considered to impact more aspects of cell behaviors (from left to right in Figure C1).

The most obvious difference between these results is that the model (12) and (13) derived in this work does not permit traveling waves for compactly supported initial conditions in u when $m_0 = 1$. This is a direct result of consistently including volume-filling effects across all the mechanisms of cell movement, such that there is always a maximum number of cells present at any point in space. The results match those of the model (C3) and (C4) when noncompactly supported initial conditions are simulated, as presented in Appendix A.

As such, the model presented in Browning et al.[35] provides a good model simplification by which to study the qualitative properties of the solutions to (12) and (13) across all parameter values when $m_0 \in [0, 1)$, with simplifications to the FKPP model also being appropriate as $\lambda \to 0^+$ and $\lambda \to \infty$.

APPENDIX D: DERIVATION OF EIGENVALUES AND EIGENVECTORS

In this section, we derive the eigenvalues of the system of ordinary differential equations (29)–(31). This system has two equilibrium points $S_1 = (1, 0, 0)$ and $S_2 = (0, 0, m_0)$, at which we want to find eigenvalues. We first find the Jacobian of the linearized system (29)–(31). To do this, we introduce the following combinations for simplicity

$$\nu = \frac{\lambda}{c}, \qquad N = \frac{1}{1 - M}, \qquad W = MU, \tag{D1}$$

so that the Jacobian is given by

$$\mathbf{J} = \begin{pmatrix} 0 & 1 & 0 \\ N(M-1+2U-3\nu^2 WU - \nu W) & -N(c+\nu W) & UN(1-\nu^2 U^2 - \nu V + N(U+M-1-\nu^2 WU)) - N^2(cV+\nu) \\ \nu M & 0 & \nu U \end{pmatrix}.$$

$$(D2)$$

Then the Jacobian at $S_2 = (0, 0, m_0)$ is

$$\mathbf{J}_{(0,0,m_0)} = \begin{pmatrix} 0 & 1 & 0 \\ \dfrac{m_0-1}{1-m_0} & \dfrac{-c}{1-m_0} & 0 \\ \dfrac{\lambda}{c}m_0 & 0 & 0 \end{pmatrix},$$

$$(D3)$$

and the Jacobian at $S_1 = (1, 0, 0)$ is

$$\mathbf{J}_{(1,0,0)} = \begin{pmatrix} 0 & 1 & 0 \\ 1 & -c & 1-\left(\dfrac{\lambda}{c}\right)^2 \\ 0 & 0 & \dfrac{\lambda}{c} \end{pmatrix}.$$

$$(D4)$$

By looking for the solutions of $\det|\mathbf{J} - \sigma\mathbf{I}| = 0$, where $\mathbf{I}$ is the identity matrix, we can find the eigenvalues of these matrices and calculate their corresponding eigenvectors. As such, at (1,0,0), the eigenvalues are $\sigma_1 = \lambda/c$, $\sigma_{2,3} = (-c \pm \sqrt{c^2+4})/2$, which have associated eigenvectors

$$\mathbf{v_1} = \left(\frac{c^2-\lambda^2}{c^2(\lambda-1)+\lambda^2}, \quad \frac{\lambda(c^2-\lambda^2)}{c(c^2(\lambda-1)+\lambda^2)}, \quad 1 \right)^T,$$

$$(D5)$$

$$\mathbf{v_{2,3}} = \left(\frac{c \pm \sqrt{c^2+4}}{2}, \quad 0, \quad 1 \right)^T.$$

$$(D6)$$

These indicate that (1,0,0) is a three-dimensional, hyperbolic, unstable saddle point since it has one negative and two positive eigenvalues.

At $(0, 0, m_0)$, $\det|\mathbf{J}_{(0,0,m_0)} - \sigma\mathbf{I}| = 0$ gives eigenvalues $\sigma_1 = 0$, $\sigma_{2,3} = (-c \pm \sqrt{c^2 - 4(1-m_0)^2})/2(1-m_0)$, showing that $(0, 0, m_0)$ is a nonhyperbolic, stable steady state, since one of these eigenvalues has zero real part. If $c^2 < 4(1-m_0)^2$, then we have a spiral at $(0, 0, m_0)$, and, otherwise, a stable node point. The corresponding eigenvectors are

$$\mathbf{w_1} = (0, 0, 1)^T,$$

$$(D7)$$

$$\mathbf{w_{2,3}} = \left(\frac{c(c \pm \sqrt{c^2 - 4(1-m_0)^2})}{2\lambda m_0(m_0-1)}, \quad \frac{c(c^2 \pm c\sqrt{c^2 - 4(1-m_0)^2} - 2(1-m_0)^2)}{2\lambda m_0(1-m_0)^2}, \quad 1 \right)^T.$$

$$(D8)$$

APPENDIX E: TRAVELING WAVE PROFILES FOR $\lambda \to 0^+$ AND $\lambda \to \infty$
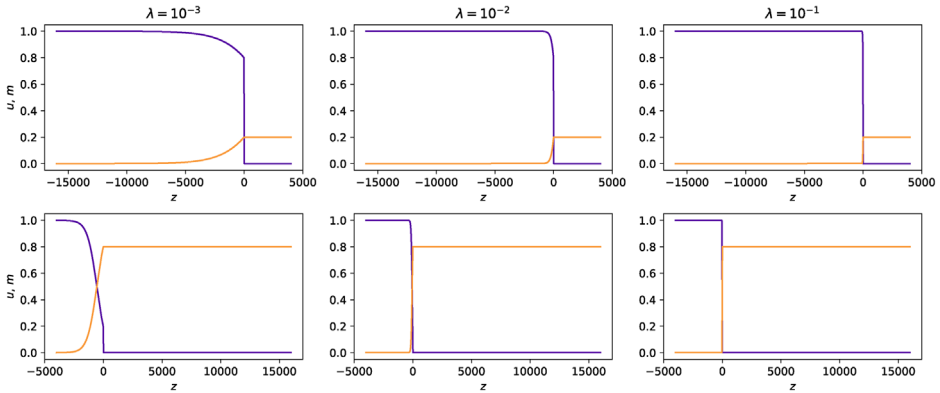

FIGURE E1   Traveling wave solutions of Equations (12) and (13) subject to the initial conditions (16) and (17), for $m_0 = 0.2$ in the top row and $m_0 = 0.8$ in the bottom row, and for rescaled ECM degradation rates $\lambda = 10^{-3}, 10^{-2}, 10^{-1}$. Cell densities are shown in purple and ECM densities in orange. Further specifics of the parameter values and the numerical methods used can be found in Appendix B.
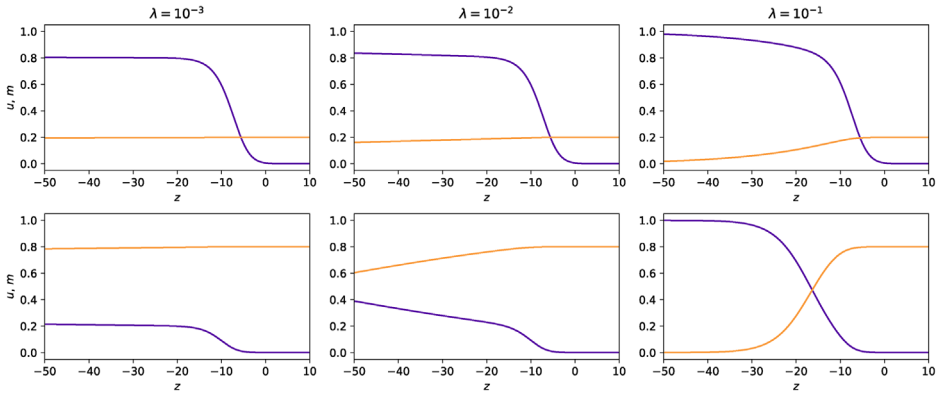

FIGURE E2   Traveling wave solutions of Equations (12) and (13) subject to the initial conditions (16) and (17), for $m_0 = 0.2$ in the top row and $m_0 = 0.8$ in the bottom row, and for rescaled ECM degradation rates $\lambda = 10^{-3}, 10^{-2}, 10^{-1}$. Cell densities are shown in purple and ECM densities in orange, zoomed in on the evolved traveling wavefront, as shown in Figure E1. Further specifics of the parameter values and the numerical methods used can be found in Appendix B.
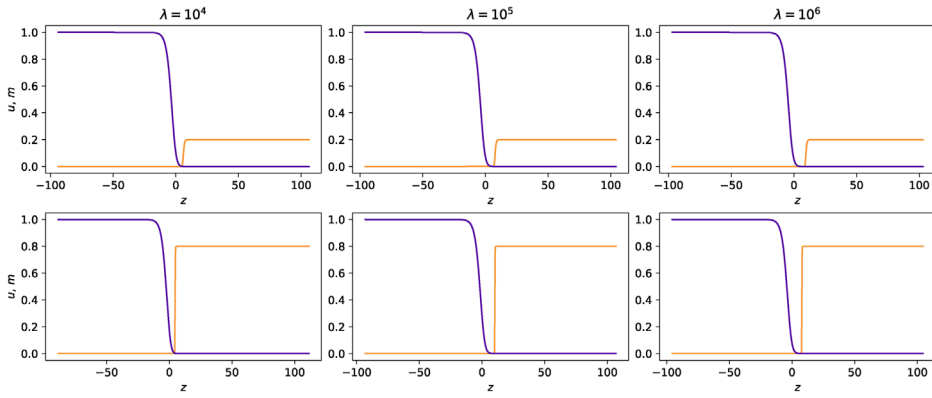
FIGURE E3 Traveling wave solutions of Equations (12) and (13) subject to the initial conditions (16) and (17), for $m_0 = 0.2$ in the top row and $m_0 = 0.8$ in the bottom row and for rescaled ECM degradation rates $\lambda = 10^4$, 10^5, 10^6. Cell densities are shown in purple and ECM densities in orange. Further specifics of the parameter values and the numerical methods used can be found in Appendix B.